Ore Geology Reviews 87 (2017) 88–99

Contents lists available at ScienceDirect

Ore Geology Reviews

journal homepage: www.elsevier.com/locate/oregeorev

Composition and characteristics of the ferromanganese crusts from the western Arctic Ocean

Natalia Konstantinova [a,b,*,1], Georgy Cherkashov [a,b], James R. Hein [c], José Mirão [d], Luís Dias [d], Pedro Madureira [e,f], Vladislav Kuznetsov [a], Fedor Maksimov [a]

[a] Saint-Petersburg State University, St. Petersburg 199034, Russia
[b] Institute for Geology and Mineral Resources of the Ocean (VNIIOkeangeologia), St. Petersburg 190121, Russia
[c] U.S. Geological Survey, Santa Cruz, CA 95060, USA
[d] The Laboratory HERCULES, University of Evora, Évora 7000-809, Portugal
[e] Estrutura de Missão para a Extensão da Plataforma Continental, Paçod'Arcos 2770-047, Portugal
[f] Universidade de Évora, Instituto de Ciências da Terra, Dep. de Geociências, Évora 7000-671, Portugal

ARTICLE INFO

Article history:
Received 13 April 2016
Received in revised form 14 August 2016
Accepted 9 September 2016
Available online 10 September 2016

Keywords:
Ferromanganese crusts
Mendeleev Ridge
Arctic Ocean

ABSTRACT

Layered ferromanganese crusts collected by dredge from a water depth range of 2770 to 2200 m on Mendeleev Ridge, Arctic Ocean, were analyzed for mineralogical and chemical compositions and dated using the excess ^{230}Th technique. Comparison with crusts from other oceans reveals that Fe-Mn deposits of Mendeleev Ridge have the highest Fe/Mn ratios, are depleted in Mn, Co, and Ni, and enriched in Si and Al as well as some minor elements, Li, Th, Sc, As and V. However, the upper layer of the crusts shows Mn, Co, and Ni contents comparable to crusts from the Atlantic and Indian Oceans. Growth rates vary from 3.03 to 3.97 mm/Myr measured on the uppermost 2 mm. Mn and Fe oxyhydroxides (vernadite, ferroxyhyte, birnessite, todorokite and goethite) and nonmetalliferous detrital minerals characterize the Arctic crusts. Temporal changes in crust composition reflect changes in the depositional environment. Crust formation was dominated by three main processes: precipitation of Fe-Mn oxyhydroxides from ambient ocean water, sorption of metals by those Fe and Mn phases, and fluctuating but large inputs of terrigenous debris.

1. Introduction

The economic interest in oceanic ferromanganese (Fe-Mn) crusts and nodules results from high grades of base, critical, and rare metals (Anikeeva et al., 2002; Hein et al., 2000; Muiños et al., 2013). Hydrogenetic Fe-Mn crusts have gained recognition as a potential future resource for a wide variety of elements such as Co, Ti, Mn, Ni, Pt, Zr, Nb, Te, Bi, Mo, W, Th, and rare earth elements plus yttrium (REY; Hein and Koschinsky, 2014). The Fe and Mn oxides form from the direct precipitation from ambient seawater and are deposited mostly on the flat tops and flanks of seamounts where oceanic currents prevent sedimentation (Anikeeva et al., 2002; Hein and Koschinsky, 2014; Melnikov, 2005).

Fe-Mn deposits are distributed globally with the largest fields in the Pacific Ocean, and smaller fields in the Atlantic and Indian Oceans. The Arctic Ocean remains a poorly explored region for deep-ocean mineral deposits. Fe-Mn deposits within the western Arctic Ocean were reported by a number of scientists (e.g., Baturin et al., 2014). In 2014, fragments of Fe-Mn crusts were sampled southwest of the study area via submersible (Fig. 1A) (Bazilevskaya and Skolotnev, 2015). Mainly 1–2 mm-thick crusts and two 30 mm-thick crusts were collected on that cruise. In 2008, 2009, and 2012, US scientists collected Fe-Mn crusts from the Chukchi Borderland that are similar in appearance and composition to those reported here (Fig. 1A) (Hein et al., 2012).

We present here data for Fe-Mn crusts collected from the western Arctic Ocean. Crusts were sampled on Mendeleev Ridge and studied in terms of morphology, mineralogy, and chemical composition, and a genetic model is proposed based on these characteristics. Our study includes a considerable number of samples containing thick (up to 50 mm) crusts. An integrated approach based on the application of different analytical techniques (i.e. ICP, ICP-MS, XRD, ED, SEM-EDX, EPMA) was used to better determine the chemical and mineral compositions of the crust samples, which then can be related to regional geological and oceanographic conditions.

2. Material and methods

Geological and geophysical studies at Mendeleev Ridge were carried out using the Russian ice breaker Kapitan Dranitzyn within the

* Corresponding author.
E-mail address: NPKonstantinova@gmail.com (N. Konstantinova).
[1] Postal address: 1, Angliysky Avenue, Saint-Petersburg, 190121, Russia.

http://dx.doi.org/10.1016/j.oregeorev.2016.09.011
0169-1368/

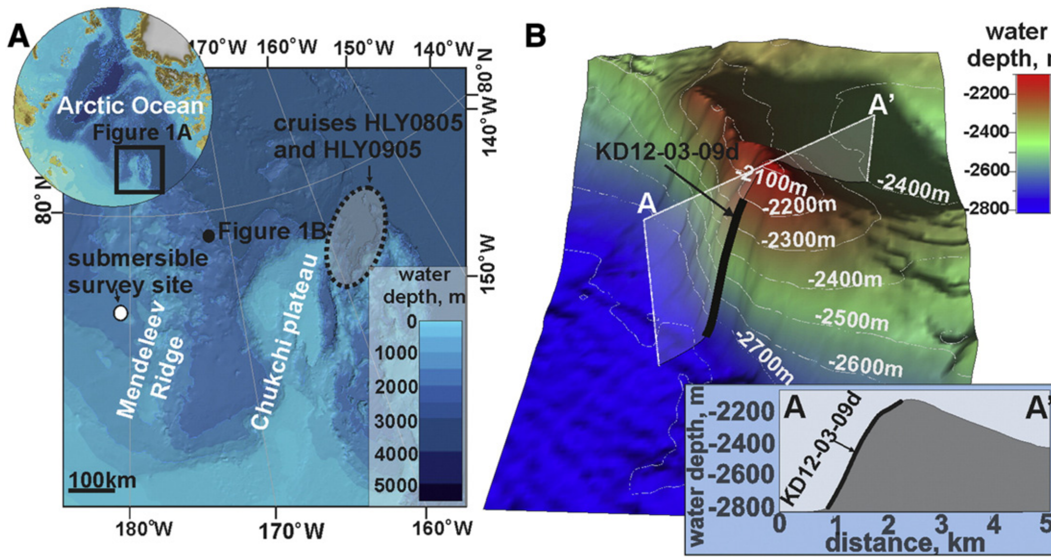

Fig. 1. Sampling Location. A (Jakobsson et al., 2012): Location of research area (inset), ellipse shows location of HLY0805 and HLY0905 cruises (USA) (Hein et al., 2012); black dot is the dredge site of the Arctic 2012 Project from which samples were obtained for this study; white dot is the area studied by submersible in 2014 (Bazilevskaya and Skolotnev, 2015); B: Bathymetric map with detailed location of dredge site from the Arctic 2012 Project (Morozov et al., 2013).

framework of the Arctic 2012 Project (Morozov et al., 2013). A dredging site was selected on the southern Mendeleev Ridge based on seafloor morphology and located on the southwestern slope of a local depression covering the depth range of 2770 to 2200 m, latitude 79° 27.0′ N and longitude 171° 59.4′ W (Fig. 1).

The dredge haul recovered rock fragments (total 500 kg) of different sizes (2–25 cm) and compositions. The major rock types are, in decreasing order: carbonate rocks (dolomite, limestone), terrigenous rocks (sandstone, siltstone, argillite), ferromanganese crusts, igneous rocks (granite, dolerite), and metamorphic rocks (quartzite, marble, schist)

Table 1
Methods applied to each sample.

Sample	Type	Interval (mm)	Methods (laboratory)
12/01	Bulk	0–50	ICP-AES (VIMS), AAS (VIMS, VNIIO), ICP-MS (VIMS)
12/02	Bulk	0–50	ICP-AES (VIMS), AAS (VIMS, VNIIO), ICP-MS (VIMS)
12/03	Bulk	0–50	ICP-AES (VIMS), AAS (VIMS, VNIIO), ICP-MS (VIMS)
12/04/01	Layer	0–5	ICP-AES (VIMS), AAS (VIMS, VNIIO), ICP-MS (VIMS), ED (IORAS), $^{230}Th_{excess}$ dating method (SPSU), XRDA (SPSU), EPMA (Geomodel, SPSU)
12/04/02	Layer	5–27	ICP-AES (VIMS), AAS (VIMS, VNIIO), ICP-MS (VIMS), ED (IORAS), XRDA (SPSU), EPMA (Geomodel, SPSU)
12/04/03	Layer	27–37	ICP-AES (VIMS), AAS (VIMS, VNIIO), ICP-MS (VIMS), ED (IORAS), XRDA (SPSU), EPMA (Geomodel, SPSU)
12/05/02	Bulk	0–50	ICP-AES (VIMS), AAS (VIMS, VNIIO), ICP-MS (VIMS)
12/06	Bulk	0–50	ICP-AES (VIMS), AAS (VIMS, VNIIO), ICP-MS (VIMS)
12/07	Bulk	0–50	ICP-AES (VIMS), AAS (VIMS, VNIIO), ICP-MS (VIMS)
12/08/01	Layer	0–3	ICP-AES (VIMS), AAS (VIMS, VNIIO), ICP-MS (VIMS), ED (IORAS), XRDA (SPSU), SEM-EDS (Hercules Lab)
12/08/02	Layer	3–17	ICP-AES (VIMS), AAS (VIMS, VNIIO), ICP-MS (VIMS), ED (IORAS), XRDA (SPSU), SEM-EDS (Hercules Lab)
12/08/03	Layer	17–24	ICP-AES (VIMS), AAS (VIMS, VNIIO), ICP-MS (VIMS), ED (IORAS), XRDA (SPSU), SEM-EDS (Hercules Lab)
12/09/01	Layer	0–3	ICP-AES (VIMS), AAS (VIMS, VNIIO), ICP-MS (VIMS), ED (IORAS), $^{230}Th_{excess}$ dating method (SPSU), XRDA (SPSU), SEM-EDS (Hercules Lab), EPMA (Geomodel, SPSU)
12/09/02	Layer	3–23	ICP-AES (VIMS), AAS (VIMS, VNIIO), ICP-MS (VIMS), ED (IORAS), XRDA (SPSU), SEM-EDS (Hercules Lab), EPMA (Geomodel, SPSU)
12/09/03	Layer	23–35	ICP-AES (VIMS), AAS (VIMS, VNIIO), ICP-MS (VIMS), ED (IORAS), XRDA (SPSU), SEM-EDS (Hercules Lab), EPMA (Geomodel, SPSU)
12/10	Bulk	0–50	ICP-AES (VIMS), AAS (VIMS, VNIIO), ICP-MS (VIMS), ED (IORAS)
12/11/01	Layer	0–1	ICP-AES (VIMS), AAS (VIMS, VNIIO), ICP-MS (VIMS), ED (IORAS)
12/11/02	Layer	1–30	ICP-AES (VIMS), AAS (VIMS, VNIIO), ICP-MS (VIMS), ED (IORAS)
12/12	Bulk	0–50	ICP-AES (VIMS), AAS (VIMS, VNIIO), ICP-MS (VIMS)
12/13	Bulk	0–50	ICP-AES (VIMS), AAS (VIMS, VNIIO), ICP-MS (VIMS), ED (IORAS)
648/01	Layer	0–5	ICP-AES (VSEGEI), AAS (VNIIO), ICP-MS (VSEGEI), SEM-EDS (Hercules Lab)
648/02	Layer	5–18	ICP-AES (VSEGEI), AAS (VNIIO), ICP-MS (VSEGEI), SEM-EDS (Hercules Lab)
648/03	Layer	18–25	ICP-AES (VSEGEI), AAS (VNIIO), ICP-MS (VSEGEI), SEM-EDS (Hercules Lab)
649	Bulk	0–50	AAS (VNIIO)
650/01	Layer	0–1	ICP-AES (VSEGEI), AAS (VNIIO), ICP-MS (VSEGEI)
650/02	Layer	1–24	ICP-AES (VSEGEI), AAS (VNIIO), ICP-MS (VSEGEI)
650/03	Layer	24–34	ICP-AES (VSEGEI), AAS (VNIIO), ICP-MS (VSEGEI)
651/01	Layer	0–3	AAS (VNIIO)
651/02	Layer	3–20	AAS (VNIIO)
651/03	Layer	20–38	AAS (VNIIO)
652	Bulk	0–50	AAS (VNIIO)
653	Bulk	0–50	AAS (VNIIO)
654	Bulk	0–50	AAS (VNIIO)
660	Bulk	0–50	AAS (VNIIO)
667	Bulk	0–50	AAS (VNIIO)
668	Bulk	0–50	AAS (VNIIO)

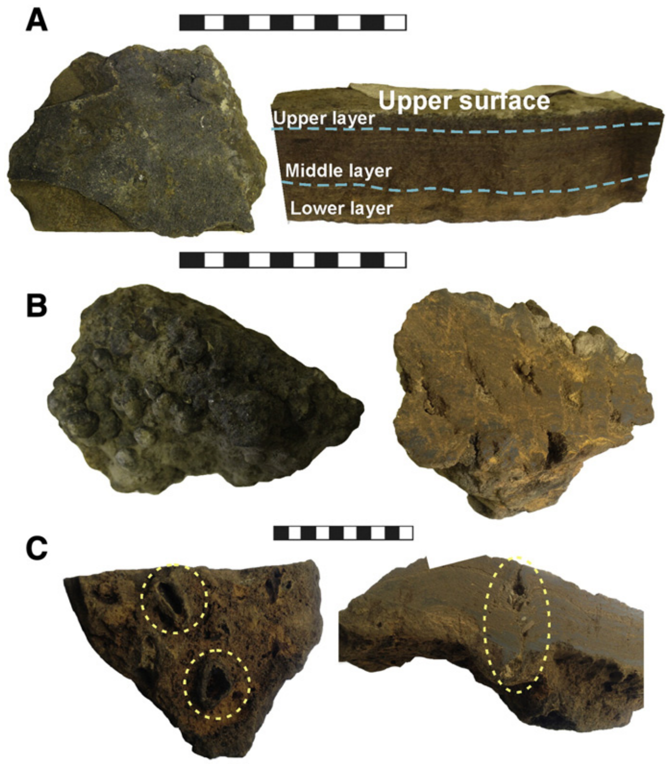

Fig. 2. Morphology of crusts. A: 12/08 sample with smooth surface texture (left) and three-layered structure (right); B: 12/03 sample with botryoidal surface structure (left) and indistinct layering (right); C: 12/04 sample with oval holes at the bottom surface (left) and void channels passing through all layers (right).

(Morozov et al., 2013). Fe-Mn crusts occur as films <1 mm thick up to 50 mm thick and represent approximately 20% by volume of the dredged material. The crusts that we analyzed range in thickness from 10 mm to 50 mm. The substrate rock for the thick (>10 mm) crusts was not recovered; Fe-Mn films and occasional thin crusts were recovered along with their substrate rock.

Twenty-three representative crusts were selected for study and seven of those crusts were split into two or three layers defined by visually distinct textural and color differences, and analyzed separately (Table 1), giving a total of 36 samples analyzed. Crust samples were studied by using a wide set of methods in several laboratories (Table 1). X-ray diffraction mineralogy was completed using a Rigaku Mini Flex II diffractometer with CoKα radiation and graphite monochromator. Mineral composition of Mn oxides and Fe hydroxides was determined using Electron microdiffraction (ED) JEM-100C microscope equipped with a built-in goniometer.

Concentrations of the major metals (Mn, Fe, Co, Ni, Cu, Pb, Zn) were determined by AAS calibrated by certified standards using a C-155 spectrometer with flame atomization. Li, Be, Sc, Cr, Zn, Ga, As, Se, Rb, Sr, Y, Mo, Rh, Pd, Cd, Sn, Sb, Te, Cs, Ba, REE, W, Ir, Pt, Tl, Pb, U, Zr, Nb, Ag, Hf, Ta, Re, and Au concentrations were measured by ICP-MS using Optima 4300 (Perkin Elmer); Na, Mg, Al, Si, P, K, Ca, and Ti by ICP-AES using Elan 6100 (Perkin Elmer). The distributions of Al, Ca, Fe, Mn, Co, Ni, Cu, Ba, Cl, K, Mg, Na, O, P, Pb, S, Si, Ti, and Zn on the surface of polished-sections were studied by SEM-EDS (Hercules Laboratory, Evora University). Electron probe microanalysis of grains was done using a scanning electron microscope (SEM; Hitachi S-3400 N) and energy dispersive X-ray (EDX) spectrometer (Oxford X-Max 20; Geomodel Center, St. Petersburg State University, operator Vladimir Shilovskich); spectra were obtained at 20 kV accelerating voltage, and 2 and 10 nA beam current for the EDX. Standards included natural minerals and pure oxides and metals. REY plots are normalized to shale (PAAS, Post-Archean Australian Shale; McLennan, 1989). The Ce anomaly was calculated as $Ce^* = 2Ce / (La + Pr)$ for PAAS-normalized values. The Pearson correlation coefficients were used to calculate coefficient matrices for the chemical data.

The $^{230}Th_{excess}$ dating method was used to determine the age and average growth rate of two crusts (Kuznetsov, 2008). This technique allows for the estimation of average growth rate only for the uppermost 2 mm of the crusts. We could not determine growth rates directly of the older layers due to the age limitation of the method that covers about 400 kyr.

3. Results and discussion

Crusts are classified as hydrogenetic and hydrothermal depending on the fluid source providing the metals. The parameters that help distinguish between hydrogenetic and hydrothermal deposits include textures, mineral and chemical compositions, and growth rates (e.g. Anikeeva et al., 2002; Hein and Koschinsky, 2014; Melnikov, 2005; Usui et al., 1989).

3.1. Textures

As a rule, the crusts have distinct layering and a smooth surface (Fig. 2A). Crusts that show a botryoidal surface and indistinct layering are less common (Fig. 2B). The top surface is easily identifiable on samples without a substrate rock by the orientation of botryoides and other structures, sediment infiltration into pore space, and remnants of attached sessile biota. The surface that was attached to the substrate rock is irregular and can show patches of the substrate rock. The six thicker crusts consistently show three layers (Fig. 2A right): a lower reddish brown layer that averages 12 mm thick; a middle brown layer that is 18 mm thick; and an upper layer that varies from dark brown to black and is 2–3 mm thick.

SEM-EDS data show that the three Fe-Mn crust layers are characterized by different microtextures that reflect different depositional styles (Fig. 3). The lower layer shows a mottled texture composed of laminated Fe-Mn oxide bodies mixed with abundant detrital grains, which form a highly porous layer. The middle layer has a laminated texture consisting of alternating Fe-Mn oxide laminae and clastic material-rich laminae. The upper layer texture shows typical botryoidal, columnar, and dendritic patterns of microlayered Fe-Mn oxides (Fig. 3; also see details in Fig. 4). All these microtextures are typical of hydrogenetic deposition of Fe-Mn phases in crusts (e.g., Hein et al., 2000).

Sample 12/04 shows void channels passing through all layers and appearing at the base of crust as oval holes. Their origin is unknown, but they could be interpreted as channels of fluid migration (Fig. 2C).

3.2. Mineral composition

The mineral compositions of Fe-Mn oxides and detrital minerals were studied by different methods. Based on X-ray and ED methods, oxide minerals consist of poorly crystalline Fe-oxyhydroxide and Mn-oxide minerals (Table 2). The predominant Mn oxide is vernadite, with less common birnessite and todorokite. Goethite and feroxyhyte were identified as the Fe-oxyhydroxides. Based on the literature, the major oxide minerals that compose crusts (Fe-bearing vernadite and Mn-bearing feroxyhyte) are considered to be characteristic of hydrogenetic precipitation (e.g. Chukhrov et al., 1990; Halbach et al. (1982); Hein et al., 1988; Usui and Someya, 1997). On the other hand, todorokite and goethite can also be produced by hydrothermal or diagenetic processes (Anikeeva et al., 2002; Bogdanova and Gorshkov, 1992; Chukhrov et al., 1990; Usui et al., 1989), but may also reflect redox conditions (Conrad et al., accepted for publication). Thus, a few samples from Mendeleev Ridge (12/10, 12/13, 12/04/02, 12/04/03) are

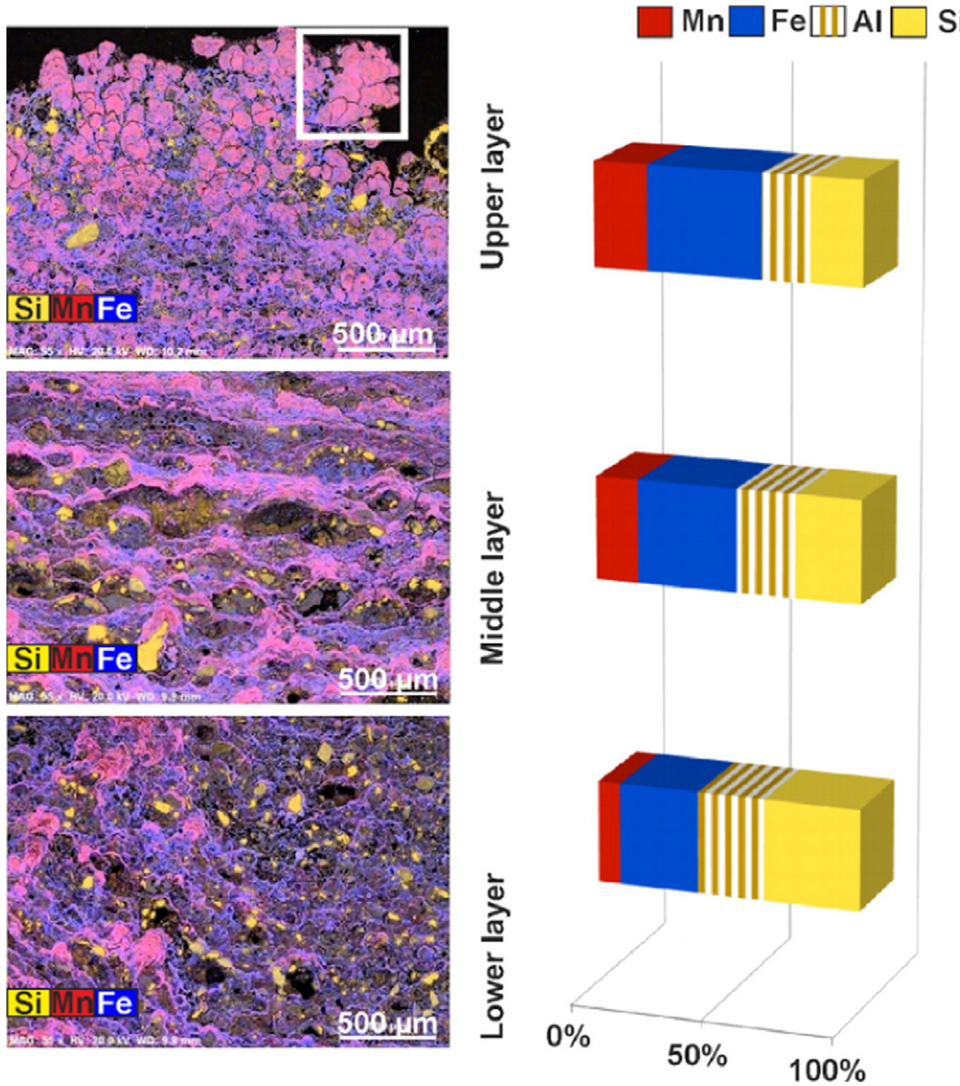

Fig. 3. SEM-EDS results: textures and chemical maps shown in the photos at the left; the mean chemical content for the areas shown the left photos are shown as bar graphs to the right. White square in top photo shows area in Fig. 4.

composed of well-crystallized goethite and lesser amounts of todorokite with 9.75 Å basal spacing, and a small amount of nonferrous vernadite.

All layers contain nonmetalliferous detrital minerals that decrease in abundance from the lower to upper layers (Fig. 3). The detrital component consist of fine-grained particles and larger mineral grains differing in roundness, size, and composition that are genetically associated with various rock types. Thus, grains of quartz, feldspar, apatite, barite, ilmenite, zircon, monazite, rutile, baddeleyite and chromite were identified by SEM-EDS (Fig. 5). As a rule, the grains are characterized by angular shapes (Fig. 5A, B, D, E), while well-rounded minerals are less common (Fig. 5A,C). A considerable difference in roundness and genesis of the

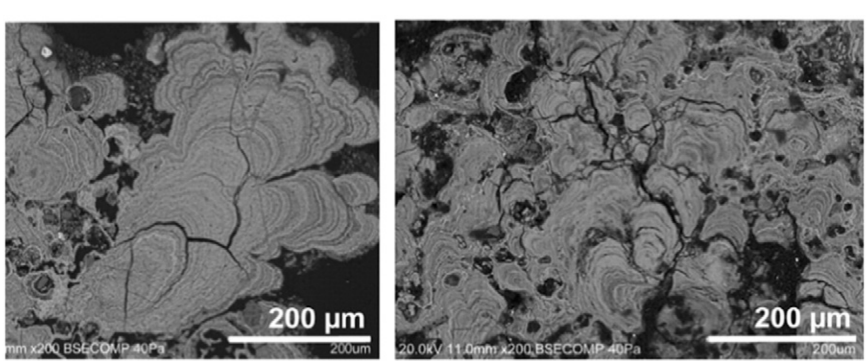

Fig. 4. SEM photomicrographs of botryoidal and dendritic patterns of laminated oxides showing typical growth columns and elongated pore spaces between branching columns; detail of the upper layer.

Table 2
Fe and Mn minerals in three crusts identified by ED.

	12/11	12/04	12/08
Upper layer	Iron-free vernadite, with a poorly ordered spectrum	Fe-bearing vernadite, feroxyhyte, goethite	Vernadite, birnessite, goethite
Middle layer	Fe-bearing vernadite, feroxyhyte, goethite	Goethite, todorokite	Vernadite
Lower layer	No lower layer	Goethite, todorokite	Fe-bearing vernadite, feroxyhyte

Table 3
Statistics for major elements (%), metals of economic potential (%), Mn/Fe and Si/Al ratios.

	Statistics	Fe	Mn	Cu	Ni	Co	Fe/Mn	Si	Al	Si/Al
All samples (N = 36)	Average	17.6	6.7	0.06	0.18	0.14	3,1	10.4	2.8	3.8
	Minimum	13.3	2.7	0.03	0.06	0.04	1,4	4.9	0.6	2.4
	Maximum	41.0	10.7	0.11	0.44	0.42	14,1	17.0	3.8	8.8
	SD	4.5	2.3	0.01	0.07	0.08	–	6.0	1.7	–
Upper layer (N = 7)	Average	17.4	7.8	0.06	0.25	0.26	2,4	9.0	2.3	3.9
	Minimum	15.3	4.2	0.05	0.09	0.08	1,6	5.70	1.8	2.7
	Maximum	20.2	10.0	0.08	0.44	0.42	3,6	12.6	3.6	4.9
	SD	2.07	2.1	0.01	0.10	0.10	–	3.4	0.9	–
Middle layer (N = 7)	Average	18.5	7.4	0.07	0.16	0.14	2,6	7.9	2.8	3.9
	Minimum	16.5	5.0	0.05	0.07	0.09	1,8	6.1	2.2	2.7
	Maximum	20.3	10.4	0.11	0.21	0.17	3,6	10.7	3.2	4.9
	SD	1.1	1.8	0.02	0.04	0.03	–	2.3	0.5	–
Lower layer (N = 6)	Average	16.7	3.8	0.05	0.09	0.07	3,5	13.4	3.3	4.1
	Minimum	15.4	2.7	0.04	0.08	0.05	1,7	11.3	2.9	3.6
	Maximum	17.6	4.6	0.07	0.11	0.08	5,6	16.5	3.7	4.5
	SD	1.1	1.0	0.01	0.02	0.02	–	2.6	0.4	–

Dash means no data, unknown, or not applicable.

mineral grains may reflect the influence of ice rafted debris in the study area. In addition, some detrital grains were likely supplied from weathering products of Mendeleev Ridge itself.

3.3. Chemical composition

The chemical composition of Fe-Mn crusts is described in the order of major elements (Si, Al, Fe, Mn) and metals traditionally considered of greatest economic potential (Co, Ni, Cu); trace elements; and REY.

3.3.1. Major elements and metals of economic potential

Fe-Mn crusts are a potential resource for a wide variety of metals such as Mn, Ni, Co and Cu (e.g., Anikeeva et al., 2002; Halbach et al., 1982; Hein et al., 2013). Mendeleev crusts show Ni and Co contents up to 0.44% and 0.42%, respectively (Table 3, Fig. 6). Table 3 shows statistics for Si, Al, Mn, Fe, Co, Ni, and Cu contents, and Fe/Mn and Si/Al ratios. Comparison with crusts from the Atlantic, Indian and Pacific Oceans (Hein et al., 2013) shows that Fe-Mn deposits of Mendeleev Ridge have the highest Fe/Mn ratios, are depleted in Mn, Co, Ni (Fig. 6), and enriched in Si and Al. The upper crust layer shows Mn, Co, and Ni contents comparable to crusts from the Atlantic and Indian Oceans.

Generally, hydrogenetic crusts from the global ocean are strongly enriched in Co and Ni, and to a lesser extent in Cu (e.g. Anikeeva et al., 2002; Hein and Koschinsky, 2014). Thus, the contents in the crusts from the Magellan Seamounts in the west Pacific average 0.54% Co, 0.41 Ni, and 0.11 Cu (Anikeeva et al., 2002), and more generally from the central Pacific Prime Crust Zone (PCZ; Hein et al., 2009), 0.67%, 0.42%, and 0.10% respectively (Hein et al., 2013). The crusts from Mendeleev Ridge are characterized by occasional high contents of Co in the upper layer (up to 0.42%), which is typical of hydrogenetic processes and is the most variable element among the potentially economic metals. High contents of Ni and low Cu in Mendeleev crusts do not per se discriminate between hydrothermal and hydrogenetic input to the crusts.

The concentrations of major elements, the Fe/Mn ratios, and Co and Ni contents show a consistent pattern. Contents of Mn, Ni, Co, Cu increase from the lower layer to the upper layer (Table 3; Figs. 3, 7). Si and Al show the opposite pattern, with maximum concentrations of Si and Al of 16.5% and 3.7% respectively. The mean Si (10.4%) and Al (2.8%) contents of the crusts analyzed here are substantially higher in comparison with crusts from other oceans (Fig. 6). The SEM-EDS results corroborate the main element variation through the three crust layers. The abundance of Mn increases with time, from the base of the section to the surface, with the concomitant decrease of Si and Al. The Fe and Mn distributions are similar even though Fe also occurs in the aluminosilicate and other detrital minerals as well as the Fe oxyhydroxide; we also infer that Fe occurs as an isomorphic phase in the manganese oxides. This inference is supported by high Fe/Mn (3.1) and high Fe/Fe + Mn (0.76) ratios. The Fe/Al + Si ratios are variable, with maximum values in the upper and middle layers (1.6), and the lower layer shows the minimum ratio (0.9); the average ratio for all layers is 1.3. Mendeleev Ridge crusts have low Fe/Al + Si ratios compared with crusts from the PCZ (3.33; Hein et al., 2013). Therefore, the Fe associated

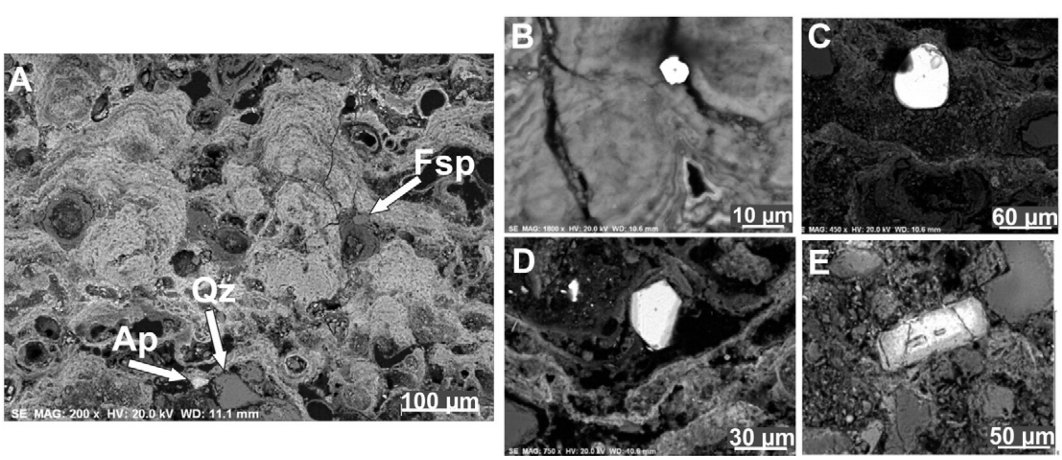

Fig. 5. SEM images of detrital minerals. Grains differ in roundness and are associated with various rock types. A: Fsp-feldspar, Ap-apatite, Qz-quartz. B: monazite; C: zircon; D: chromite; E: apatite.

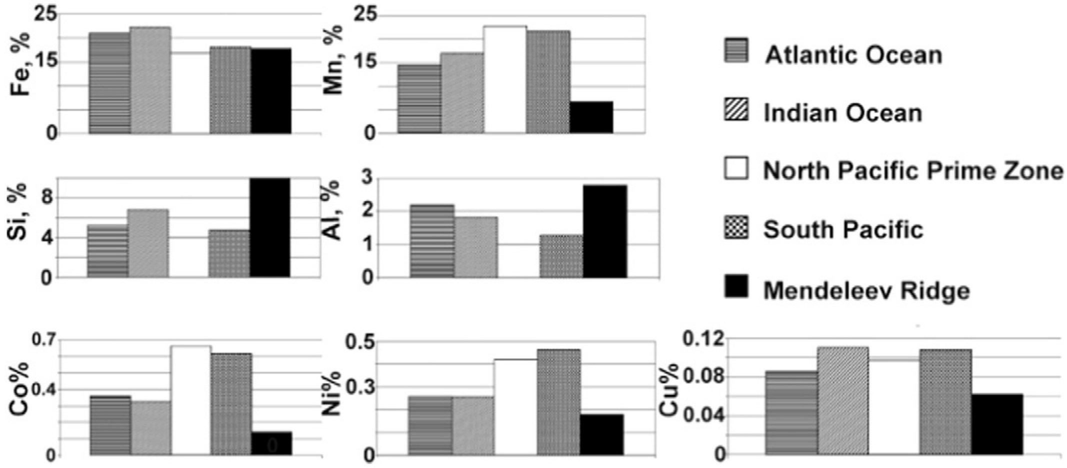

Fig. 6. Comparison of chemical composition of Fe-Mn crusts from Mendeleev Ridge with crusts from other oceans (Hein et al., 2013).

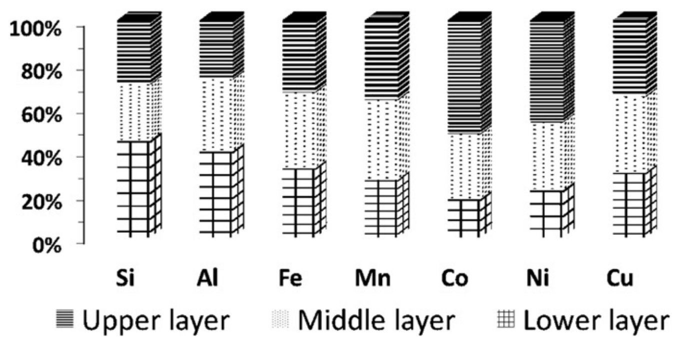

Fig. 7. Layer by layer distribution of major metals in Fe-Mn crusts.

with the detritus and with the iron hydroxide do not have the same vertical distributions through the crust stratigraphic sections.

Based on literature data, bulk samples of hydrogenetic crusts show Fe/Mn ratios of approximately 1.0 ± 0.3 (e.g. Hein et al., 2000; Dubinin, 2006; Hein and Koschinsky, 2014). This value changes dramatically for hydrothermal deposits because of the fractionation of iron and manganese: from Fe/Mn ~4600 for bulk samples of hydrothermal ironstone to Fe/Mn = 0.002 for bulk samples of hydrothermal manganese (Glasby, 2000; Hein et al., 1994, 1997). Hydrothermal ironstone deposits exhibit low contents of most trace elements (Hein et al., 1994, 1997), whereas manganese hydrothermal deposits can be enriched in one or more of Ni, Mo, Li, Cr, and Zn (Hein and Koschinsky, 2014). The crusts from Mendeleev Ridge give a high average Fe/Mn ratio, 3.1, and even a higher ratio for the lower crust layer, 3.5 (Table 3). This is due to the fact that a large amount of iron is supplied by the terrigenous detritus, confirming its significant effect on crust formation.

3.3.2. Trace elements

Table 4 shows statistics for the trace elements. The Fe-Mn crusts contain high concentrations of several trace elements, Li (up to 310 ppm), Th (up to 87 ppm), Cs (up to 3.3 ppm in the lower layer), As (up to 770 ppm), Y (up to 290 ppm), V (up to 1060 ppm), and Sc (up to 66 ppm). Comparison of Sc, Th, As, Li, and V concentrations in the Mendeleev Ridge Fe-Mn deposits and Fe-Mn crusts from the Atlantic, Indian and Pacific Oceans (Hein et al., 2013) are shown in Fig. 8. The Mendeleev Ridge crusts are markedly enriched in Li, As, and Sc in comparison with the other trace elements, and the Th and V concentrations are comparable to those of Atlantic and Indian Oceans crusts. The enrichments of V, Y and Zr reflect in part the detrital component.

3.3.3. Rare earth elements plus yttrium

Table 5 shows REY statistics for bulk samples and for the different layers. The mean total REY is 0.17% and the maximum total REY is 0.25%. By comparison, the REY content of hydrogenetic crusts from PCZ is approximately 0.25% (Hein et al., 2013).

Changes in the REY content are important for reconstruction of the Fe-Mn deposit evolution. REY_{SN} (SN = shale normalized) patterns may show anomalies for La, Ce, Eu, Gd and Y. Except for these anomalies, REY_{SN} patterns are smooth functions of ionic radius (Bau et al., 2014). All samples from Mendeleev Ridge have a similar REY distribution, with Ce anomalies as high as 2.7 and weak negative Y anomalies (Fig. 9A). As a rule, hydrogenetic crusts exhibit distinct positive Ce anomalies (Fig. 9B). Ce is subject to oxidation on the Mn-oxide surface subsequent to sorption from solution (e.g. Murray and Dillard, 1979; Dubinin, 2006). For comparison, Fig. 9B shows the REY distributions for Fe-Mn deposits formed by different processes: hydrogenetic, diagenetic and hydrothermal (McLennan, 1989; Bau et al., 2014).

Table 4
Statistics for trace elements (ppm) of 26 crust samples from Mendeleev Ridge.

	Li	Be	Sc	Cr	Zn	Ga	As	Se	Rb	Sr	Y	Mo	V	Sn
Average	102	6.0	50	39	355	14	574	8.7	43	587	199	276	908	4.8
Minimum	31	3.0	26	11	230	8.6	378	1.8	20	150	93	70	683	0.6
Maximum	310	8.0	66	66	480	21	770	17	68	880	290	460	1060	7.4
SD	71	1.2	11	11	57	3.5	112	3.9	13	170	55	101	148	1.6
	Sb	**Te**	**Cs**	**Ba**	**W**	**Tl**	**Pb**	**Bi**	**Th**	**U**	**Zr**	**Nb**	**Hf**	**Ta**
Average	52	13	2.1	519	44	83	269	3.2	51	10	487	46	8.6	0.7
Minimum	27	0.9	0.9	330	9.1	33	15	0.1	1.9	3.6	49	3.0	1.0	0.1
Maximum	92	36	3.3	590	65	130	560	9.4	87	13	770	100	13	1.3
SD	17	9.8	0.6	55	13	30	141	2.7	20	1.8	183	20	3.3	0.2

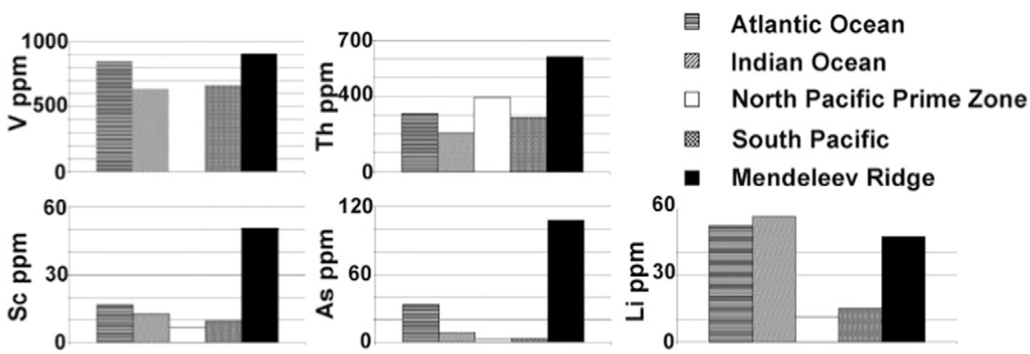

Fig. 8. Comparison of Sc, Th, As, and Li average concentrations in the Fe-Mn crusts from the Mendeleev Ridge, and from the Atlantic, Indian, and Pacific Oceans (Hein et al., 2013).

The Ce_{SN}/Ce^*_{SN} versus Nd and Ce_{SN}/Ce^*_{SN} vs Y_{SN}/Ho_{SN} diagrams were developed to identify the genesis of marine ferromanganese deposits (Bau et al., 2014). In Fig. 10A, the hydrothermal Fe and Mn precipitates show negative to no Ce anomalies at low Nd concentrations (<12 mg kg^{-1}), but Ce_{SN}/Ce_{SN}^* ratios tend to increase with increasing Nd concentration. Hydrogenetic Fe–Mn crusts typically show positive Ce anomalies and high Nd concentrations (>100 mg kg^{-1}) (Bau et al., 2014). Samples of Mendeleev Ridge crusts plot within the hydrogenetic field (Fig. 10A). In a bivariate diagram of Ce_{SN}/Ce_{SN}^* versus Y_{SN}/Ho_{SN} (Fig. 10B), a similar separation between the different groups can be observed. Hydrothermal deposits clearly stand out and form a group with positive Y anomalies ($Y_{SN}/Ho_{SN} > 1$) and Ce_{SN}/Ce_{SN}^* ratios tend to increase with decreasing Y_{SN}/Ho_{SN} ratios. All hydrogenetic deposits are characterized by negative Y anomalies ($Y_{SN}/Ho_{SN} < 1$; Bau et al., 2014). The crusts from Mendeleev Ridge plot in the area located between all three typical genetic types of Fe-Mn marine deposits, but unlike hydrothermal and diagenetic deposits, the Mendeleev crusts show a positive correlation between Ce_{SN}/Ce^*_{SN} and Y_{SN}/Ho_{SN}.

3.4. Interelement relationships

Fe-Mn crusts consist of three main phases: (1) Mn-oxide and (2) Fe-oxyhydroxide composing the metal-oxide framework, and (3) silica-aluminosilicate. Some of the remaining elements have positive correlation with the representative elements of each phase (Mn, Fe, Si and Al). Table 6 shows the correlation coefficient matrix for 25 Fe–Mn crust samples from Mendeleev Ridge. Bolded data reflects correlations at a >99% confidence level. Mn has positive correlations coefficients with Ni, Co, and Th (0.81, 0.81, 0.72 respectively); and Fe with W, Be, and Sr. Both Mn and Fe have positive correlation coefficients with Cu, Se, Sn, REY, and each other. Copper correlates with about equal significance with both Mn and Fe, with coefficients of +0.59 and +0.55 respectively. A different pattern is found for silica-aluminosilicate phases. Si and Al show significant positive correlation coefficients with K, Li, Rb, Cs, and each other.

3.5. Dating

The $^{230}Th_{excess}$ method uses the radioactive decay of the excess activity of ^{230}Th over that of the parent uranium. Tables 7 and 8 show that the $^{230}Th_{excess}$ specific activity in samples from both crusts decreases gradually from the surface downward as expected from radioactive decay and therefore the method can be applied for dating (Ivanovich and Harmon, 1992; Kuznetsov, 2008).

On the basis of the relationship between the $^{230}Th_{excess}$ specific activity in the sublayers 0–0.4 mm and 0.9–1.4 mm, we calculated the average growth rate of 3.03 ± 0.28 mm/Ma for crust 12/09. This allowed us to estimate the age at the base of the 0–1.4 mm layer to be 380 ± 30 ka. The average growth rate is calculated to be 3.97 ± 0.62 mm/Ma for crust 12/04 based on the relationship between the $^{230}Th_{excess}$ specific activity in sublayers 0–0.5 mm and 1.5–2.0 mm. The estimated age is 440 ± 60 ka for the base of layer 0–2.0 mm.

We did not analyze deeper crust sublayers due to the closeness of $^{230}Th_{excess}$ activity to the radioactive equilibrium with the parent uranium in the lowermost analyzed sublayers. The calculated ages are close to the age limit of the method, about 400 ka.

The growth rates of 3.03 ± 0.28 mm/Ma and 3.97 ± 0.62 mm/Ma compare with those obtained by the Be isotope method for three crusts from the adjacent Chukchi plateau, which for the youngest (upper

Table 5
The statistics for REY contents in crusts (ppm).

	Statistics	La	Ce	Pr	Nd	Sm	Eu	Gd	Tb	Dy	Y	Ho	Er	Tm	Yb	Lu	ΣREY
All samples (N = 26)	Average	150	913	41	162	41	10	48	7	42	203	8	22	3	21	3	1674
	Minimum	84	460	23	94	24	6	26	4	24	110	5	13	2	12	2	889
	Maximum	210	1400	59	240	60	14	70	11	60	290	12	30	4	30	5	2495
	SD	46	306	12	47	12	3	13	2	11	52	2	6	1	6	1	–
Upper layer (N = 6)	Average	180	1040	49	194	49	12	56	9	50	229	10	26	4	25	4	1937
	Minimum	110	640	29	120	30	8	35	6	32	170	6	16	2	16	2	1222
	Maximum	210	1400	59	240	59	14	69	10	60	290	12	30	4	28	4	2489
	SD	37	253	11	43	11	2	12	2	10	40	2	5	1	5	1	–
Middle layer (N = 6)	Average	181	1171	50	193	50	12	57	9	50	238	10	26	4	25	4	2080
	Minimum	150	1000	42	160	41	11	48	8	43	190	8	23	3	21	3	1751
	Maximum	210	1400	57	225	60	14	70	11	59	260	12	30	4	30	5	2447
	SD	23	158	6	26	8	1	8	1	6	24	2	3	0	3	1	–
Lower layer (N = 5)	Average	113	644	30	123	32	8	37	6	31	110	6	17	2	16	2	1177
	Minimum	86	500	23	94	24	6	26	4	24	200	5	13	2	12	2	1021
	Maximum	130	810	34	140	35	9	41	7	36	160	7	19	3	18	3	1452
	SD	19	130	4	20	5	1	6	1	5	46	1	2	0.3	3	1	–

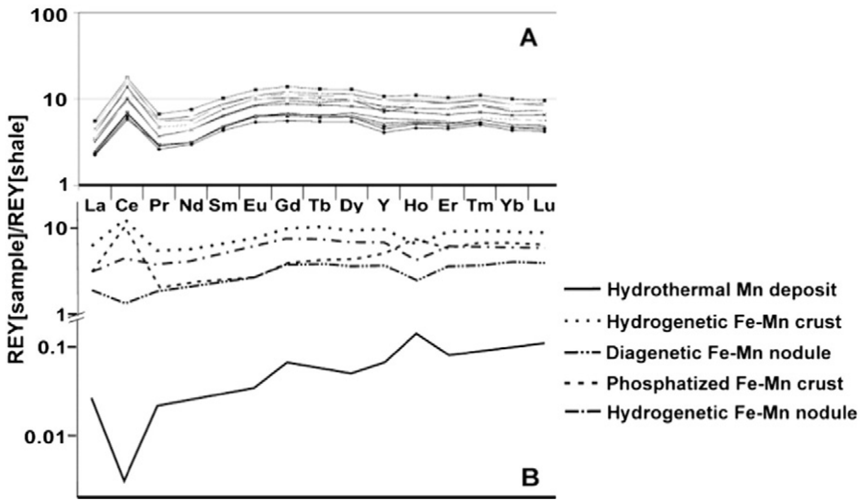

Fig. 9. Shale-normalized REY patterns (PAAS); A: Mendeleev Ridge samples; B: different marine Fe-Mn deposits (McLennan, 1989; Bau et al., 2014).

5 mm) layer of each crust vary from 2.18 to 8.22 mm/Myr (Dausmann et al., 2015).

4. Fe-Mn crust formation

Our results help constrain the metal sources and formation history of the Fe-Mn crusts from Mendeleev Ridge. The most informative genetic parameters for crust chemical and mineral compositions are Co, Ni, Cu, and REY contents, Fe/Mn ratios, and Fe and Mn minerals (Anikeeva et al., 2002; Dubinin, 2006; Hein and Koschinsky, 2014; Kuhn et al., 1998; Manheim and Lane-Bostwick, 1988).

Hydrogenetic crusts commonly have botryoidal and dendritic textures and slow growth rates (e.g. Hein et al., 2000; Anikeeva et al., 2002; Melnikov, 2005; Dubinin, 2006; Kuznetsov, 2008; Hein and Koschinsky, 2014). These characteristics are typical for the upper layer of Mendeleev crusts with growth rates of 3.03–3.97 mm/Myr (Tables 7,8). The age for the base of the crusts uppermost 3 mm layer, calculated from average growth rates and average thickness of 3 mm are 0.91 to 1.19 Myr. These data indicate that the oxides were sourced from seawater and therefore have a hydrogenetic origin. Unlike deep-water open-ocean crusts, the Mendeleev crusts show the presence of high amounts of nonmetalliferous detritus of terrigenous origin.

Data for each of the three layers analyzed separately indicate a temporal change in the conditions of crust formation (Figs. 2A, 3). Textural features between the terrigenous component and metal oxides highlight the variability of input of terrigenous detritus with time. Besides a general decrease in detrital input with time, the laminated structure described for the middle layer reflects a fluctuating input of terrigenous debris against the background of slow precipitation of Fe and Mn oxides (Fig. 3). Formation of the lower layer was associated with the intense input of terrigenous material as evidenced by the mottled texture and maximum Al and Si contents (Fig. 3, Table 3). These changes in detrital input reflect predominantly changes in weathering conditions on the adjacent continents and, based on variations in rounding of grains, that transport was by rivers and sea ice. In addition, we suggest that clastic minerals may also have been supplied to the crusts by weathering of Mendeleev Ridge rocks (Rekant et al., 2013).

5. Conclusions

Study of crusts from Mendeleev Ridge revealed their morphology, texture, mineral and chemical compositions, and processes of formation. The morphological and textural features of the samples show that the crusts have a three-layered structure and each layer has its own microtexture.

As a whole, the Mendeleev samples are depleted in elements of greatest economic interest compared to the crusts from the Pacific Prime Crust Zone, though the metal contents in the upper layer of the Mendeleev crusts are often comparable. Generally, the Arctic Ocean crusts have comparable metal contents with Fe-Mn crusts from the

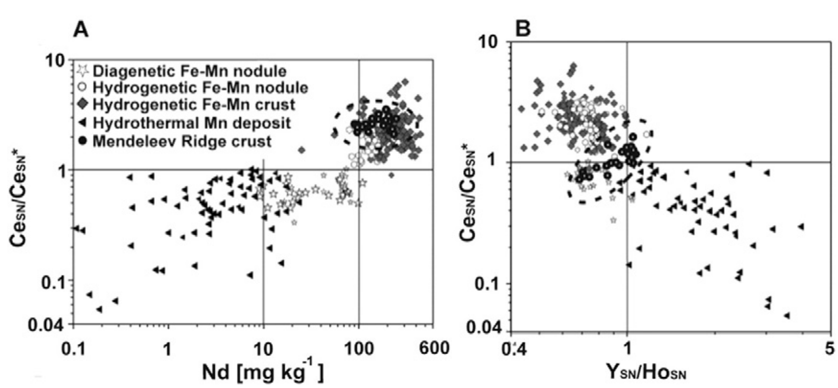

Fig. 10. Marine Fe–Mn oxyhydroxide deposits for (A) Ce_{SN}/Ce_{SN}^* vs Nd concentration and (B) Ce_{SN}/Ce_{SN}^* ratio vs Y_{SN}/Ho_{SN} (Bau et al., 2014); SN is shale normalized to Post-Archean Australian Shale, PAAS (McLennan, 1989); Ce* = Ce anomaly ($Ce_{SN}^* = 0.5La_{SN} + 0.5\ Pr_{SN}$).

Table 6
Correlation coefficient matrix for 25 Fe–Mn crust samples.

	Na	Mg	Al	Si	P	K	Ca	Ti	Fe	Mn	Cu	Ni	Co	Li	Be	Sc	Cr	Zn	Ga	As	Se	Rb
Mg	0.0519																					
Al	**0.5406**	-0.4436																				
Si	0.3613	-0.4194	**0.8244**																			
P	0.4883	0.2923	0.4849	0.2029																		
K	0.4080	-0.4755	**0.9297**	**0.9259**	0.3527																	
Ca	0.3560	0.4264	-0.2812	-0.1476	0.1527	-0.2876																
Ti	0.4251	0.3032	0.1439	0.0760	0.4274	0.1458	0.0913															
Fe	-0.4442	0.1173	**-0.6798**	**-0.8081**	-0.2392	**-0.6717**	-0.0298	-0.1106														
Mn	**-0.5961**	0.2691	**-0.8757**	-0.7926	**-0.5524**	**-0.8822**	0.1013	-0.3426	**0.5355**													
Cu	-0.3592	0.4482	**-0.6891**	**-0.6441**	-0.1818	**-0.6720**	-0.0888	0.0295	**0.5469**	**0.5875**												
Ni	-0.4101	0.3910	**-0.8222**	**-0.6598**	-0.4169	**-0.7793**	0.1463	-0.2173	0.4177	**0.8077**	**0.6328**											
Co	-0.3775	0.5044	**-0.9238**	**-0.6867**	-0.4193	**-0.8808**	0.4064	-0.0848	0.4160	**0.8076**	**0.6287**	**0.8037**										
Li	0.2958	-0.4157	**0.7170**	**0.6597**	0.0922	**0.6201**	-0.3679	-0.1979	**-0.6735**	-0.4535	-0.3683	-0.4330	**-0.6088**									
Be	-0.2146	0.0082	-0.2730	**-0.6635**	0.1245	-0.4228	-0.0936	0.0008	**0.7197**	0.2877	0.1514	0.0126	0.0607	-0.4764								
Sc	0.0651	0.0609	0.1053	-0.3623	0.4159	-0.0855	-0.3423	0.3739	0.3857	-0.0575	0.1862	-0.1965	-0.2379	-0.1391	**0.7416**							
Cr	-0.1030	0.0168	0.4438	0.4993	0.1186	**0.5503**	-0.4148	0.2167	-0.3761	-0.3798	-0.3504	-0.3543	-0.4999	0.2934	-0.2340	0.0622						
Zn	0.0334	**0.6079**	-0.4430	**-0.6863**	0.2756	**-0.6205**	0.1986	0.3478	0.4687	0.3426	**0.6118**	0.3309	0.4539	-0.4430	0.4539	**0.5926**	-0.3556					
Ga	-0.5764	**-0.5616**	-0.0704	-0.0128	**-0.5925**	0.0330	-0.5811	-0.4622	0.1719	0.2930	-0.1351	0.1261	-0.1196	0.1139	0.1610	-0.0448	0.3010	**-0.5157**				
As	0.2102	0.4292	-0.1556	-0.4681	**0.5331**	-0.3247	0.2008	0.3649	0.4615	-0.0308	0.3777	-0.0121	0.1380	-0.4199	**0.5585**	**0.6728**	-0.3532	**0.8473**	-0.6280			
Se	-0.4753	-0.0621	**-0.7026**	**-0.6306**	**-0.6800**	-0.6736	0.0238	-0.2762	**0.5336**	**0.7617**	0.3753	**0.5979**	**0.5458**	-0.4018	0.2778	-0.1013	-0.3399	0.0684	0.4999	-0.2560		
Rb	0.3872	-0.4243	**0.9111**	**0.8143**	0.4845	**0.9357**	-0.3275	0.2953	**-0.5654**	**-0.8740**	**-0.6512**	**-0.7974**	**-0.8731**	0.4744	-0.2066	0.1760	**0.5497**	-0.4137	-0.0095	-0.0882	**-0.7249**	
Sr	-0.0042	**0.6322**	**-0.6109**	**-0.8110**	0.1821	**-0.7705**	0.4295	0.1791	**0.5952**	0.4683	0.5037	0.4048	**0.6019**	**-0.6448**	**0.5784**	0.4136	**-0.5465**	**0.8858**	-0.4921	**0.8019**	0.1935	-0.5880
Y	-0.1566	**0.6001**	**-0.7368**	**-0.9091**	0.0477	**-0.8801**	0.3489	0.1447	**0.6480**	**0.6436**	**0.5991**	**0.5357**	**0.7038**	**-0.6781**	**0.6149**	0.4153	**-0.5237**	**0.8517**	-0.3173	**0.6788**	0.3913	**-0.7094**
Mo	0.3263	0.4555	-0.0716	-0.4689	**0.5128**	-0.3439	0.2573	0.2629	0.2732	0.0397	0.2239	-0.0450	0.1024	-0.2431	**0.5184**	**0.5962**	-0.4086	**0.7963**	-0.6564	**0.8668**	-0.1927	-0.1489
Cd	0.3297	0.4251	-0.1179	-0.4411	0.3149	-0.4368	0.3048	0.1492	0.0728	0.1768	0.1888	0.0892	0.2088	0.0055	0.3232	0.3920	-0.4370	**0.6883**	-0.5042	**0.5798**	0.0174	-0.3025
Sn	**-0.7139**	0.1096	**-0.8465**	**-0.6863**	**-0.6136**	**-0.7291**	-0.0325	-0.2726	**0.6538**	**0.8221**	**0.5263**	**0.6928**	**0.6836**	**-0.5447**	0.3286	-0.0425	-0.1908	0.1263	**0.5157**	-0.1536	**0.8151**	**-0.7431**
Sb	-0.0326	**0.6851**	**-0.6181**	**-0.6232**	0.1515	**-0.6732**	0.4039	0.2439	0.2989	0.5086	**0.6212**	**0.5872**	**0.7236**	**-0.5172**	0.1731	0.2006	-0.3890	**0.7890**	-0.4512	**0.5410**	0.1306	-0.5630
Te	0.2989	**0.6811**	-0.2641	-0.3016	0.4476	-0.3288	**0.5378**	0.4560	0.1872	-0.0050	0.4373	0.0887	0.3671	-0.3743	0.0709	0.2256	-0.3331	**0.7628**	-0.8631	**0.7823**	-0.2773	-0.2230
Cs	0.0931	**-0.5973**	**0.6770**	**0.6061**	0.2164	**0.7774**	-0.4679	0.0646	-0.2274	-0.6386	-0.5464	-0.4877	**-0.7940**	0.2833	-0.0674	0.1439	0.5041	**-0.5255**	0.3526	-0.2221	-0.3839	**0.8190**
Ba	0.0877	0.2924	-0.0905	-0.2818	0.4698	-0.1569	0.3029	0.0980	0.4213	-0.1078	0.0855	-0.1182	0.0084	-0.4557	0.4809	0.3619	-0.3380	0.5060	-0.4631	**0.7508**	-0.2365	0.0334
La	-0.3680	0.4288	**-0.8801**	**-0.9363**	-0.2473	**-0.9301**	0.2944	-0.0928	**0.8095**	**0.7558**	**0.6091**	**0.6398**	**0.7749**	**-0.7710**	**0.5945**	0.1783	**-0.5995**	**0.6315**	-0.0869	0.4774	**0.5900**	**-0.8269**
Ce	-0.1520	**0.5342**	**-0.6890**	**-0.8679**	0.0785	**-0.8127**	0.3400	0.1030	**0.7075**	**0.5652**	**0.5803**	0.4370	**0.6307**	**-0.7180**	**0.6297**	0.3735	**-0.5728**	**0.7812**	-0.3865	**0.7224**	0.3144	**-0.6604**
Pr	-0.3285	0.4036	**-0.8750**	**-0.9247**	-0.2633	**-0.9271**	0.3411	-0.0974	**0.7902**	**0.7589**	**0.5926**	**0.6277**	**0.7796**	**-0.7514**	**0.5574**	0.1351	**-0.6617**	**0.6079**	-0.1174	0.4559	**0.5993**	**-0.8406**
Nd	-0.3697	0.4095	**-0.8848**	**-0.9443**	-0.2600	**-0.9366**	0.2962	-0.1197	**0.8090**	**0.7850**	**0.5978**	**0.6640**	**0.7802**	**-0.7643**	**0.5872**	0.1709	**-0.6014**	**0.6168**	-0.0424	0.4386	**0.6275**	**-0.8393**
Sm	-0.4389	0.3350	**-0.9013**	**-0.9288**	-0.3684	**-0.9366**	0.2537	-0.2054	**0.7873**	**0.8459**	**0.5829**	**0.6928**	**0.7820**	**-0.7255**	**0.5499**	0.0931	**-0.5958**	**0.5128**	0.0727	0.3061	**0.7126**	**-0.8671**
Eu	-0.3110	0.4159	**-0.8513**	**-0.9443**	-0.2209	**-0.9257**	0.3111	-0.0968	**0.7814**	**0.7690**	**0.5866**	**0.6422**	**0.7403**	**-0.7347**	**0.5807**	0.1875	**-0.6370**	**0.6229**	-0.0873	0.4537	**0.6171**	**-0.8270**
Gd	-0.4239	0.3528	**-0.8996**	**-0.9482**	-0.3453	**-0.9457**	0.2395	-0.1836	**0.7856**	**0.8491**	**0.6009**	**0.7055**	**0.7765**	**-0.7117**	**0.5707**	0.1357	**-0.5808**	**0.5349**	0.0809	0.3148	**0.7245**	**-0.8726**
Tb	-0.4071	0.3959	**-0.8958**	**-0.9508**	-0.3013	**-0.9490**	0.2675	-0.1592	**0.7789**	**0.8296**	**0.6114**	**0.6841**	**0.7841**	**-0.7307**	**0.5791**	0.1516	**-0.5898**	**0.5736**	0.0132	0.3712	**0.6755**	**-0.8662**
Dy	-0.3670	0.4274	**-0.8925**	**-0.9545**	-0.2742	**-0.9490**	0.2757	-0.1237	**0.7618**	**0.8200**	**0.6257**	**0.7195**	**0.7820**	**-0.7226**	**0.5495**	0.1528	**-0.5773**	**0.5921**	0.0053	0.3640	**0.6934**	**-0.8692**
Ho	-0.4695	0.3388	**-0.9182**	**-0.9310**	-0.4087	**-0.9476**	0.2056	-0.2043	**0.7450**	**0.8835**	**0.6197**	**0.7466**	**0.8035**	**-0.6901**	0.5022	0.0813	**-0.5308**	0.4880	0.1502	0.2154	**0.7877**	**-0.8974**
Er	-0.3914	0.4465	**-0.9127**	**-0.9304**	-0.3142	**-0.9558**	0.2746	-0.1156	**0.7054**	**0.8525**	**0.6618**	**0.7215**	**0.8272**	**-0.7117**	0.4750	0.1002	**-0.5611**	**0.5707**	0.0028	0.3035	**0.7214**	**-0.8939**
Tm	-0.3668	0.4463	**-0.9053**	**-0.9223**	-0.3006	**-0.9520**	0.2933	-0.0778	**0.6984**	**0.8308**	**0.6698**	**0.7083**	**0.8275**	**-0.7158**	0.4749	0.1154	**-0.5771**	**0.5938**	-0.0313	0.3330	**0.7096**	**-0.8808**
Yb	-0.3986	0.4064	**-0.9027**	**-0.9392**	-0.3142	**-0.9485**	0.2492	-0.0926	**0.7433**	**0.8349**	**0.6582**	**0.6995**	**0.7934**	**-0.7081**	**0.5231**	0.1449	**-0.5378**	**0.5690**	0.0458	0.3120	**0.7428**	**-0.8775**
Lu	-0.4366	0.3694	**-0.8938**	**-0.9355**	-0.3425	**-0.9338**	0.1958	-0.1479	**0.7353**	**0.8579**	**0.6511**	**0.7000**	**0.7736**	**-0.6845**	**0.5425**	0.1529	**-0.5148**	**0.5173**	0.1241	0.2555	**0.7699**	**-0.8720**
W	-0.0461	0.2118	-0.3265	**-0.7117**	0.1186	**-0.5537**	0.1283	-0.1627	**0.6095**	0.4018	0.2865	0.1486	0.1886	-0.3536	**0.7351**	0.4778	**-0.5214**	**0.5827**	-0.1790	**0.6018**	0.2628	-0.4231
Tl	0.3276	**0.5883**	-0.1249	-0.3567	0.4954	-0.3092	0.3519	0.4618	0.1439	0.0398	0.3367	0.0153	0.1853	-0.2449	0.2743	0.4905	-0.3192	**0.8077**	**-0.7688**	**0.8055**	-0.2269	-0.1352
Pb	-0.1115	**0.6606**	**-0.7932**	**-0.7202**	-0.0356	**-0.7900**	0.4816	0.1794	**0.5946**	**0.5091**	**0.6986**	**0.6159**	**0.8012**	**-0.7197**	0.2211	0.0479	**-0.5636**	**0.7288**	-0.4972	**0.6061**	0.2704	**-0.7112**
Bi	0.2308	**0.6512**	-0.3571	-0.3576	0.3462	-0.3852	**0.5455**	0.4301	0.2977	0.0534	0.4789	0.1367	0.4211	-0.4727	0.1007	0.1864	-0.3859	**0.7333**	**-0.8161**	**0.7710**	-0.1957	-0.2829
Th	-0.3493	0.4546	**-0.9312**	**-0.7637**	-0.3478	**-0.8820**	0.4117	-0.1142	0.6302	**0.7251**	**0.7003**	**0.7442**	**0.9215**	**-0.6809**	0.2149	-0.1450	**-0.6153**	0.5030	-0.1616	0.2991	0.5368	**-0.8805**
U	0.2370	**0.5795**	-0.1752	-0.4144	0.3625	-0.4310	0.3343	0.0887	-0.0842	0.2775	0.1590	0.2395	0.3204	-0.0764	0.1774	0.2011	-0.3486	**0.5809**	-0.4905	0.3922	0.0048	-0.3566
Zr	0.1111	-0.0095	0.2203	-0.1253	0.3999	0.0642	-0.3262	0.2548	0.1683	-0.1388	0.0613	-0.2104	-0.2812	-0.0816	0.4283	**0.6711**	0.1029	0.2852	0.0062	0.3704	-0.0701	0.2547
Nb	0.0511	**0.7286**	**-0.5936**	**-0.5865**	0.2127	**-0.6365**	0.4747	0.3643	0.4095	0.3543	**0.6282**	0.4468	**0.6741**	-0.6278	0.1705	0.2141	-0.4180	**0.8382**	**-0.6299**	**0.7057**	0.0614	-0.5008
Hf	-0.3368	-0.4037	0.0486	-0.1345	-0.1086	0.0444	**-0.5596**	-0.1621	0.3184	0.1201	0.0369	-0.0592	-0.2386	-0.0813	0.3985	0.3729	0.1670	-0.1674	**0.6061**	-0.1473	0.3325	0.1062
Ta	-0.0361	0.2910	-0.3035	-0.1924	0.0530	-0.2534	0.1004	0.2501	0.2000	0.1817	0.4518	0.2698	0.3542	-0.3218	-0.0788	0.0878	-0.0635	0.2976	-0.1458	0.1719	0.1477	-0.2099

	Sr	Y	Mo	Cd	Sn	Sb	Te	Cs	Ba	La	Ce	Pr	Nd	Sm	Eu	Gd	Tb	Dy	Ho	Er	Tm	Yb
Y	**0.9592**																					
Mo	**0.8020**	**0.6801**																				
Cd	**0.6860**	0.6279	**0.8081**																			
Sn	0.2526	0.4654	-0.2770	-0.1779																		
Sb	**0.7626**	**0.7863**	0.4571	0.4318	0.3180																	
Te	**0.7185**	**0.5937**	**0.6621**	**0.5148**	-0.1548	**0.7063**																
Cs	**-0.6469**	**-0.7030**	-0.3661	**-0.5654**	-0.3944	**-0.6511**	-0.4987															
Ba	**0.6275**	0.4561	**0.6539**	0.3386	-0.1685	0.2818	**0.5661**	-0.0404														
La	**0.8448**	**0.9011**	0.4478	0.3726	**0.6516**	**0.6180**	0.3786	**-0.6500**	0.4191													
Ce	**0.9364**	**0.9429**	**0.7265**	**0.5357**	0.3795	**0.6670**	**0.5989**	**-0.6298**	**0.5446**	**0.9058**												
Pr	**0.8357**	**0.8879**	0.4519	0.3901	**0.6340**	**0.6043**	0.3885	**-0.6740**	0.4071	**0.9910**	**0.9059**											
Nd	**0.8265**	**0.8939**	0.4152	0.3597	**0.6815**	**0.6346**	0.3449	**-0.6464**	0.3899	**0.9914**	**0.8853**	**0.9869**										
Sm	**0.7393**	**0.8340**	0.3118	0.3010	**0.7415**	**0.5617**	0.2199	**-0.6368**	0.2997	**0.9719**	**0.8247**	**0.9739**	**0.9857**									
Eu	**0.8355**	**0.8986**	0.4698	0.4301	**0.6331**	**0.6122**	0.3558	**-0.6473**	0.4100	**0.9778**	**0.8987**	**0.9860**	**0.9842**	**0.9777**								
Gd	**0.7467**	**0.8530**	0.3177	0.3295	**0.7569**	**0.5845**	0.2225	**-0.6443**	0.2777	**0.9685**	**0.8231**	**0.9661**	**0.9832**	**0.9954**	**0.9769**							
Tb	**0.7877**	**0.8817**	0.3728	0.3607	**0.7225**	**0.6123**	0.2830	**-0.6683**	0.3213	**0.9815**	**0.8624**	**0.9781**	**0.9888**	**0.9928**	**0.9849**	**0.9961**						
Dy	**0.7855**	**0.8833**	0.3633	0.3819	**0.7202**	**0.6411**	0.2919	**-0.6645**	0.3036	**0.9678**	**0.8418**	**0.9622**	**0.9812**	**0.9825**	**0.9795**	**0.9926**	**0.9923**					
Ho	**0.6737**	**0.8096**	0.2185	0.2719	**0.8151**	**0.5745**	0.1530	**-0.6507**	0.1566	**0.9321**	**0.7603**	**0.9270**	**0.9548**	**0.9789**	**0.9422**	**0.9869**	**0.9764**	**0.9805**				
Er	**0.7477**	**0.8668**	0.3188	0.3577	**0.7477**	**0.6526**	0.2877	**-0.7220**	0.2243	**0.9435**	**0.8231**	**0.9435**	**0.9600**	**0.9709**	**0.9602**	**0.9798**	**0.9802**	**0.9861**	**0.9845**			
Tm	**0.7632**	**0.8786**	0.3384	0.3808	**0.7301**	**0.6668**	0.3229	**-0.7291**	0.2480	**0.9431**	**0.8311**	**0.9431**	**0.9566**	**0.9631**	**0.9580**	**0.9733**	**0.9760**	**0.9831**	**0.9749**	**0.9965**		
Yb	**0.7356**	**0.8616**	0.2986	0.3563	**0.7652**	**0.6217**	0.2664	**-0.6879**	0.2140	**0.9402**	**0.8078**	**0.9349**	**0.9559**	**0.9659**	**0.9527**	**0.9796**	**0.9767**	**0.9862**	**0.9856**	**0.9915**	**0.9903**	
Lu	**0.6880**	**0.8322**	0.2547	0.3134	**0.8009**	**0.5880**	0.1882	**-0.6631**	0.1683	**0.9204**	**0.7755**	**0.9129**	**0.9392**	**0.9599**	**0.9340**	**0.9767**	**0.9699**	**0.9767**	**0.9886**	**0.9859**	**0.9807**	**0.9926**
W	**0.7304**	**0.6948**	**0.7760**	**0.6176**	0.1206	0.2749	0.2686	-0.3673	**0.5751**	**0.6859**	**0.7842**	**0.6962**	**0.6756**	**0.6522**	**0.7290**	**0.6471**	**0.6696**	**0.6437**	**0.5630**	**0.5887**	**0.5832**	**0.5848**
Tl	**0.7433**	**0.6372**	**0.8777**	**0.7291**	-0.2605	0.5849	0.8266	-0.4092	**0.5868**	0.3587	**0.6409**	0.3734	0.3206	0.2212	0.3857	0.2317	0.2892	0.2891	0.1388	0.2749	0.3084	0.2432
Pb	**0.8380**	**0.8212**	0.4693	0.3751	0.4134	**0.7811**	**0.7497**	**-0.6748**	0.4483	**0.8229**	**0.8256**	**0.8267**	**0.8007**	**0.7311**	**0.7925**	**0.7264**	**0.7598**	**0.7673**	**0.6887**	**0.7609**	**0.7768**	**0.7407**
Bi	**0.7304**	**0.6106**	**0.6230**	0.4523	-0.0677	0.6696	0.9801	-0.4906	0.5826	0.4574	**0.6462**	0.4746	0.4175	0.3029	0.4321	0.2975	0.3559	0.3568	0.2239	0.3501	0.3828	0.3316
Th	**0.6740**	**0.7381**	0.1794	0.1953	**0.6761**	**0.6828**	0.4420	**-0.7225**	0.1766	**0.8630**	**0.7207**	**0.8649**	**0.8535**	**0.8370**	**0.8143**	**0.8316**	**0.8424**	**0.8389**	**0.8341**	**0.8486**	**0.8479**	**0.8379**
U	**0.6268**	**0.6054**	**0.6821**	**0.7906**	-0.1061	**0.6041**	0.4410	**-0.6035**	0.2474	0.3598	**0.5109**	0.3695	0.3707	0.3286	0.4275	0.3546	0.3866	0.4110	0.3222	0.4168	0.4188	0.3634
Zr	0.1455	0.1603	0.3865	0.2092	-0.1283	0.0097	0.0068	0.2286	0.2196	-0.0127	0.1911	-0.0244	0.0346	-0.0066	0.0578	0.0082	0.0075	0.0243	0.0018	0.0278	0.0358	0.0388
Nb	**0.8254**	**0.7870**	**0.5781**	0.4540	0.2134	**0.8690**	0.8623	**-0.6127**	0.4711	**0.6403**	**0.7559**	**0.6418**	**0.6403**	**0.5393**	**0.6295**	**0.5403**	**0.5801**	**0.5997**	**0.5108**	0.6144	**0.6361**	**0.5860**
Hf	-0.2221	-0.0861	-0.1701	-0.3006	0.3062	-0.2865	**-0.5331**	0.3690	-0.1180	-0.0063	-0.0330	-0.0190	0.0585	0.1111	0.0522	0.1169	0.0764	0.0748	0.1646	0.0947	0.0755	0.1191
Ta	0.1845	0.2512	0.0063	-0.0278	0.2691	0.4378	0.3266	-0.2160	-0.0129	0.1652	0.2274	0.1806	0.2349	0.1979	0.2036	0.2020	0.1943	0.2306	0.2519	0.3003	0.3136	0.2878

	Lu	W	Tl	Pb	Bi	Th	U	Zr	Nb	Hf
W	**0.5772**									
Tl	0.1893	**0.5410**								
Pb	**0.6809**	0.4030	**0.5505**							
Bi	0.2529	0.2981	**0.7908**	**0.8133**						
Th	**0.8114**	0.3270	0.2070	**0.8857**	**0.5276**					
U	0.3451	0.5005	**0.6482**	0.3521	0.3397	0.2093				
Zr	0.0519	0.3164	0.2384	-0.1134	-0.0382	-0.2955	0.1418			
Nb	**0.5218**	0.3326	**0.6869**	**0.9016**	**0.8678**	**0.6905**	0.4578	0.1490		
Hf	0.1815	0.1541	-0.3561	-0.3380	-0.5141	-0.2337	-0.2739	**0.7221**	-0.2634	
Ta	0.2696	-0.1101	0.1294	0.3740	0.3234	0.2874	0.0100	0.5194	**0.5805**	0.3575

Bolded values reflect values above zero point of correlation for 25 at the 99% confidence level (0.505)

Table 7
Results of radiochemical analysis of the crust sample 12/09.

Sub-layer, mm	^{238}U dpm/g	^{234}U dpm/g	$^{234}U/^{238}U$	^{230}Th dpm/g	^{232}Th dpm/g	$^{230}Th_{excess}$ dpm/g
0–0.4	9.30 ± 0.85	11.32 ± 0.93	1.22 ± 0.14	141.93 ± 6.89	35.28 ± 2.18	130.61 ± 6.95
0.4–0.9	7.78 ± 0.65	8.90 ± 0.68	1.14 ± 0.12	43.05 ± 1.57	28.26 ± 1.15	34.15 ± 1.71
0.9–1.4	9.88 ± 0.81	11.36 ± 0.87	1.15 ± 0.12	18.63 ± 1.71	26.39 ± 2.17	7.26 ± 1.92
1.4–1.9	10.07 ± 0.55	14.56 ± 0.68	1.45 ± 0.10	15.63 ± 1.54	27.77 ± 2.25	–

Dash means no data available; dpm/g = decays/min/g.

Table 8
Results of radiochemical analysis of the crust sample 12/04.

Sub-layer, mm	^{238}U dpm/g	^{234}U dpm/g	$^{234}U/^{238}U$	^{230}Th dpm/g	^{232}Th dpm/g	$^{230}Th_{excess}$ dpm/g
0–0.5	6.37 ± 0.24	8.09 ± 0.27	1.27 ± 0.06	54.95 ± 2.15	24.44 ± 1.22	46.86 ± 2.16
0.5–1.0	7.30 ± 0.42	7.88 ± 0.43	1.08 ± 0.08	20.35 ± 1.09	22.59 ± 1.17	12.47 ± 1.17
1.0–1.5	6.31 ± 0.61	7.74 ± 0.66	1.23 ± 0.15	20.11 ± 0.59	20.91 ± 0.60	12.36 ± 0.89
1.5–2.0	7.32 ± 0.35	10.51 ± 0.42	1.44 ± 0.08	11.95 ± 0.66	17.70 ± 0.83	1.45 ± 0.78

dpm/g = decays/min/g.

Indian and Atlantic Oceans, and in addition have remarkably high contents of Sc, Th, Li, V, and As.

Mn has significant positive correlation coefficients with Ni, Co, and Th whereas Si has significant positive coefficients with Al, K, Li, Rb, and Cs.

The composition of the crusts shows high amounts of nonmetalliferous detrital minerals, that vary from layer to layer and have a terrigenous source. Transportation of the detrital minerals was by both rivers and sea ice. We suggest that clastic minerals may also have been supplied to the crust by weathering of Mendeleev Ridge rocks. This diverse supply of clastic material is typical of the early stages of crust formation and decreased markedly to the present.

Therefore, crust formation was dominated by three main factors: precipitation of Fe-Mn oxides from ambient ocean water, sorption of metals by those Fe and Mn phases, and fluctuating but large inputs of terrigenous material.

Growth rates of the uppermost 2 mm of the two crusts dated using excess ^{230}Th vary from 3.03 mm/Myr to 3.97 mm/Myr. The base of the upper layer (average thickness 3 mm) ranges in age from 0.9 to 1.2 Myr.

It is noteworthy that a considerable amount of Fe-Mn crusts discovered during recent Russian and USA expeditions in this part of the Arctic have similar textures and compositions, especially high contents of Li, Zr, V, Y and Sc, suggesting regional development of these metal deposits, which differ significantly from crusts reported from other parts of the global ocean.

Acknowledgements

We thank V.V. Shilovskich (Geomodel), V.P. Ruban, Dr. N.V. Platonova, Dr. E.N. Perova and A.V. Firstova from St. Petersburg State University; Dr. B.G. Vanshtein from VNIIOkeangeologia, P. Serov from CAGE for their help and analytical expertise. We are grateful to Dr. G. Novikov and Dr. O. Bogdanova from P.P. Shirshov Institute of Oceanology for performing the EM diffraction analyses. This study was partly funded and supported by projects 3.37.135.2014 and 18.37.141.2014 of St. Petersburg State University and the Scholar Program of St. Petersburg State University and Banco Santander, S.A.

Appendix 1. Acronyms list

Acronym	Full name
AAS	Atomic Absorption Spectroscopy
ED	Electron microdiffraction
EPMA	Electron Probe Microanalysis
EDX	Energy dispersive X-ray
FMC	Ferromanganese Crust
ICP-AES	Inductively Coupled Plasma Atomic Emission Spectroscopy
ICP-MC	Inductively Coupled Plasma Mass Spectrometry
IORAS	P.P. Shirshov Institute of Oceanology of the Russian Academy of Sciences
PAAS	Post-Archean Australian Shale
SD	Standard deviation
SEM-EDS	Scanning Electron Microscopy – Energy Dispersive Spectroscopy
SPSU	St. Petersburg State University
VIMS	Institute of mineral resources
VNIIO	Institute for Geology and Mineral Resources of the Ocean
VSEGEI	A.P. Karpinsky Russian Geological Research Institute
XRD	X-Ray Diffraction

References

Anikeeva, L., Andreev, S., Kazakova, V., Aleksandrov, P., Zadornov, M., Kuznetsov, V., Petuchov, S., Kulikov, N., Torochov, M., Chernomordik, A., Burskiy, A., 2002. Cobalt-rich Ores of World Ocean. VNIIOkeangeologia, St. Petersburg (in Russian with English abstract).

Baturin, G.N., Dubinchuk, V.T., Ivanov, G.I., Siraev, A.I., 2014. A specific type of Fe-Mn mineralization on the Arctic seafloor. Dokl. Earth Sci. 458 (2), 1191–1196.

Bau, M., Schmidt, K., Koschinsky, A., Hein, J.R., Kuhn, T., Usui, A., 2014. Discriminating between different genetic types of marine ferro-manganese crusts and nodules based on rare earth elements and yttrium. Chem. Geol. 381, 1–9.

Bazilevskaya, E.S., Skolotnev, G.S., 2015. Fe–Mn nodules of the Mendeleev Ridge. Arctic Ocean. Dokl. Earth Sci. 464 (2), 1015–1017.

Bogdanova, O.Y., Gorshkov, A.I., 1992. Mineralogy of low-temperature ferromanganese deposits from TAG hydrothermal field. Nauka 160–172 (in Russian).

Chukhrov, F.V., Gorshkov, A.I., Drits, V.A., Dubnina, G.A., 1990. Genesis of oceanic crusts and nodules as indicated by the crystal-chemistry of the manganese oxides. Int. Geol. Rev. 32 (3), 260–270.

Conrad, T., Hein, J.R., Paytan, A., Clague, D.A., 2016. Formation of Fe-Mn crusts within a continental margin environment. Ore Geol. Rev. 87, 25–40.

Dausmann, V., Frank, M., Siebert, C., Christl, M., Hein, J.R., 2015. The evolution of climatically driven weathering inputs into the western Arctic Ocean since the late Miocene: radiogenic isotope evidence. Earth Planet. Sci. Lett. 419, 111–124.

Dubinin, A.V., 2006. Rare Earth Elements in the Ocean. Nauka, Moscow (in Russian with English abstract).

Glasby, G.P., 2000. Manganese: predominant role of nodules and crusts. Mar. Geochem. 335–372.

Halbach, P., Manheim, F.T., Otten, P., 1982. Co-rich ferromanganese depsoits in the marginal seamount regions of the Central Pacific Basin—results of the Midpac '81. Erzmetall 35, 447–453.

Hein, J.R., Koschinsky, A., 2014. Deep-ocean ferromanganese crusts and nodules. In: Holland, H.D., Turekian, K.K. (Eds.), Treatise on Geochemistry, second edition vol. 13. Oxford, Elsevier, pp. 273–291 (Chapter 11).

Hein, J.R., Schwab, W.G., Davis, A.S., 1988. Cobalt- and platinum-rich ferromanganese crusts and associated substrate rocks from the Marshall Islands. Mar. Geol. 78, 255–283.

Hein, J.R., Yeh, H.-W., Gunn, S.H., Gibbs, A.E., Wang, C.-H., 1994. Composition and origin of hydrothermal ironstones from central Pacific seamounts. Geochim. Cosmochim. Acta 58, 179–189.

Hein, J.R., Koschinsky, A., Halbach, P., Manheim, F.T., Bau, M., Kang, J.-K., Lubick, N., 1997. Iron and manganese oxide mineralization in the Pacific. In: Nicholson, K., Hein, J.R., Bühn, B., Dasgupta, S. (Eds.), Manganese Mineralization: Geochemistry and Mineralogy of Terrestrial and Marine Deposits. Geological Society of London Special Publication No. 119, London, pp. 123–138.

Hein, J.R., Koschinsky, A., Bau, M., Manheim, F.T., Kang, J.-K., Roberts, L., 2000. Cobalt-rich ferromanganese crusts in the Pacific. In: Cronan, D.S. (Ed.), Handbook of Marine Mineral Deposits. CRC Press, Boca Raton, Florida, pp. 239–279.

Hein, J.R., Conrad, T.A., Dunham, R.E., 2009. Seamount characteristics and mine-site model applied to exploration- and mining-lease-block selection for cobalt-rich ferromanganese crusts. Mar. Georesour. Geotechnol. 27, 160–176.

Hein, J.R., Klofas, J., Mizell, K., Conrad, T.A., 2012. Rare-metal-rich ferromanganese mineral deposits from the western Arctic Ocean. Abstracts, 41st Underwater Mining Institute, 15–20 October 2012, Shanghai China, pp. 1–3 p. Hein.

Hein, J.R., Mizell, K., Koschinsky, A., Conrad, T.A., 2013. Deep-ocean mineral deposits as a source of critical metals for high- and green-technology applications: comparison with land-based resources. Ore Geol. Rev. 51, 1–14.

Ivanovich, M., Harmon, R.S. (Eds.), 1992. Uranium-series Disequilibrium: Applications to Earth, Marine and Environmental Sciences, 2nd ed. Clarendon Press, Oxford, p. 902.

Jakobsson, M., Mayer, L.A., Coakley, B., Dowdeswell, J.A., Forbes, S., Fridman, B., Hodnesdal, H., Noormets, R., Pedersen, R., Rebesco, M., Schenke, H.-W., Zarayskaya, Y.A., Accettella, D., Armstrong, A., Anderson, R.M., Bienhoff, P., Camerlenghi, A., Church, I., Edwards, M., Gardner, J.V., Hall, J.K., Hell, B., Hestvik, O.B., Kristoffersen, Y., Marcussen, C., Mohammad, R., Mosher, D., Nghiem, S.V., Pedrosa, M.T., Travaglini, P.G., Weatherall, P., 2012. The International Bathymetric Chart of the Arctic Ocean (IBCAO) version 3.0. Geophys. Res. Lett. http://dx.doi.org/10.1029/2012GL052219.

Kuhn, T., Bau, M., Blum, N., Halbach, P., 1998. Origin of negative Ce anomalies in mixed hydrothermal-hydrogenetic Fe-Mn crusts form the Central Indian Ridge. Earth Planet. Sci. Lett. 163, 207–220.

Kuznetsov, V.Y., 2008. Radiohronology of Quaternary Deposits. Comilfo, St. Petersburg (in Russian with English abstract).

Manheim, F.T., Lane-Bostwick, C.M., 1988. Cobalt in ferromanganese crusts as a monitor of hydrothermal discharge on the Pacific sea floor. Nature 335, 59–62.

McLennan, S.M., 1989. Rare earth elements in sedimentary rocks; influence of provenance and sedimentary processes. Rev. Mineral. Geochem. 21, 169–200.

Melnikov, M.E., 2005. Cobalt-rich Manganese Crust Deposits. FGUGP GNTS Yuzhmorgeologiya, Gelendzhik (in Russian).

Morozov, A.F., Petrov, O.V., Shokalsky, S.P., Kashubin, S.N., Kremenetskiy, A.A., Shkatov, M.Y., Kaminsky, V.D., Gusev, E.A., Grikurov, G.E., Rekant, P.V., Shevchenko, S.S., Sergeev, S.A., Shatov, V.V., 2013. New geological data confirming the continental nature of the Central Arctic uplifts area. Reg. Geol. Metallogeny 53, 34–55.

Muiños, S.B., Hein, J.R., Frank, M., Monteiro, J.H., Gaspar, L., Conrad, T., Garcia Pereira, H., Abrantes, F., 2013. Deep-sea Fe-Mn crusts from the northeast Atlantic Ocean: composition and resource considerations. Mar. Georesour. Geotechnol. 31 (1), 40–70.

Murray, J.W., Dillard, J.G., 1979. The oxidation of cobalt(II) adsorbed on manganese dioxide. Geochim. Cosmochim. Acta 43, 781–788.

Rekant, P., Mirolubova, E., Andreeva, I., Smirnova, L., 2013. Mineralogy of the bottom sediment from Lomonosov Ridge and Mendeleev Rise as a possible proxy to evaluation of the source rock. Problemi Arktiki i Antarktiki 4 (98), 79–95.

Usui, A., Someya, M., 1997. Distribution and composition of marine hydrogenetic and hydrothermal manganese deposits in the northwest Pacific. In: Nicholson, K., Hein, J.R., Bühn, B., Dasgupta, S. (Eds.), Manganese Mineralization: Geochemsitry and Mineralogy of Terrestial and Marine Deposits. Geological Society of London Special Publication 119, London, pp. 177–198.

Usui, A., Melin, T.A., Nohara, M., Yuasa, M., 1989. Structural stability of marine 10 Å manganates from the Ogasawara (Bonin) Arc: implication for low-temperature hydrothermal activity. Mar. Geol. 86, 41–56.